Appl. Magn. Reson. 22, 115−131 (2002)

Determination of Differential Quantum Yields in Solution by Electron Paramagnetic Resonance Spectroscopy

S. L. Quiroga, M. S. Churio, and L. J. Perissinotti

Department of Chemistry, University of Mar del Plata, Mar del Plata, Argentina

Received May 23, 2001; revised January 13, 2002

Abstract. Quantitative kinetic studies on the photochemistry of paramagnetic species in solution may be carried out by electron paramagnetic resonance (EPR) spectroscopy. A cylindrical cell can be used as photochemical reactor, but the internal diameter should be less than 1.7 mm in order to achieve the resonance of an aqueous sample in an X-band (9–10 GHz) spectrometer. In this paper we present a detailed analysis of the fractions of incident light that are reflected, transmitted and absorbed by a liquid solution in a quartz cylindrical cell placed in the optical cavity of an X-band EPR spectrometer. Since the photolysis cell is irradiated perpendicularly to its axis, variable angles of incidence have been considered to calculate the transmission and reflection coefficients from Fresnel equations. Polarization of light has been also taken into account in the evaluation of the coefficients. The procedure proposed here is adequate for the evaluation of the absorbed light in the determination of quantum yields. The continuous photolysis at 366 nm of symmetric chlorine dioxide (OClO) in aqueous solution was considered as an example. The initial differential quantum yield obtained for OClO photodecomposition in aqueous solution was $\Phi_{366} = 0.55 \pm 0.04$.

1 Introduction

Photochemical kinetic studies in solution may be carried out by electron paramagnetic resonance (EPR) measurements, by registering the concentration of the paramagnetic species within the cavity of the spectrometer while the sample is irradiated continuously or by flash. Flat cells as well as the recently developed flow-cylindrical cells [1] are suitable for EPR experiments on high-dielectric samples. However, some problems may arise for quantitative photochemical work. For instance, full irradiation of the sample is not possible in a flat cell within an EPR optical cavity, consequently rising diffusion processes.

We found that a cylindrical cell from commercial quartz tubing is adequate for EPR quantitative photochemical studies. The internal diameter of the cell must be kept small enough to allow for the resonance of the sample if aqueous solutions are used (inner diameter (i.d.) of about 1.7 mm in an X-band spectrometer).

Table 1. Comparison between irradiation conditions of different flat cells supplied by Wilmad and the cylindrical cell used in this work. The samples are placed within a TE_{103} optical cavity of an X-band EPR spectrometer. The light reaches the sample through a 4 by 11 mm optical path.

Cell	Flat section				Sample volume (μl)	Sample volume within the EPR cavity (μl)	Irradiated volume (μl)
	Length (mm)	Thickness (mm)	Internal width (mm)	Volume (μl)			
Flat WG-813*	60	0.30	~8.8	~150	~600	~60	~13
Flat WG-808*	51	0.50	~3.2	~100	~250	~37	~18
Cylindrical	Internal diameter ~1.7 mm				~25	~25	~25

* Part Number according to Wilmad catalog nr. 852.

For an EPR optical cavity with a 4 by 11 mm optical path, less than 50% of the sample volume in the cavity is irradiated when usual flat cells are employed (see the last two columns in Table 1). In consequence, practical difficulties for photochemical work may arise from diffusion between the irradiated and nonirradiated portions of the sample. Particularly, if photodecomposition of a radical species is studied, the nonirradiated portion of the sample in the flat cell may originate a significant background signal. The use of cylindrical cells override this kind of complications. In fact, 25 μl of a liquid sample can be fully irradiated when contained in a 1.7 mm i.d. cylindrical cell.

Studies of light transmission and reflection on cells with plane parallel windows have been already carried out [2–4]. These cells are the most common design for photochemical work, since the light beams impinge at normal incidence. However, to our knowledge, there is no similar study on other designs including cylindrical cells.

In this work, a complete analysis of reflection, transmission and absorption of light in a cylindrical photochemical cell is shown. Although the problem seems to be extremely complex, it is notably simplified by the geometric properties of the system. The mathematical treatment developed here can be used to evaluate the absorbed photon flow P_a (Einsteins $\cdot s^{-1}$) by a sample in a cylindrical cell which is irradiated perpendicularly to its axis, representing a significant contribution to the study of photolysis in aqueous solution by EPR spectroscopy. As an example, the absorbed photon flow P_a in the photodecomposition of aqueous chlorine dioxide (OClO) at 366 nm was evaluated.

OClO solutions undergo complete photodecomposition in a few minutes by irradiation with conventional light sources in the near ultraviolet (UV). Although studies on the photolysis of OClO have increased since it was determined as one of the main processes related to the destruction of the stratospheric ozone, most of the works on this topic refer to the primary processes [5–15]:

$$OClO + h\nu \rightarrow Cl + O_2 \ (10\%), \tag{1}$$

$$OClO + h\nu \rightarrow ClO + O \ (90\%). \tag{2}$$

The partitioning of the reaction channels and the cage recombination processes in liquid solution are solvent-dependent. In water, the reported distribution among the two channels is indicated in parentheses [11]. Two allowed mechanisms are possible for reaction (1): direct dissociation or isomerization to ClOO and subsequent dissociation into $Cl + O_2$. In water solution, 95% of the Cl is produced from the isomerization pathway [8]. Primary products in reaction (2) are recombined to OClO within the solvent cage. At 366 nm the cage escape of the fragments is about 7% [14]. Photodecomposition of OClO in aqueous solution results in the production of HCl and $HClO_3 \cdot Cl_2$, and O_2 are minor products. Neither the final products nor the radical intermediates (Cl, O, ClO and ClOO) absorb significantly at 366 nm and at their concentrations in this system [13–15].

Once the absorbed photon flow is evaluated, the differential or instantaneous quantum yield Φ_d can be calculated:

$$\Phi_d = -\frac{V\mathrm{d}C/\mathrm{d}t}{P_a}, \tag{3}$$

where $\mathrm{d}C/\mathrm{d}t$ ($\mathrm{mol} \cdot \mathrm{l}^{-1}\mathrm{s}^{-1}$) is the photodecomposition rate when a V volume (liters) of an aqueous solution of OClO is irradiated at 366 nm.

2 Experimental Section

2.1 Chemicals

Concentrated stock solutions of OClO ca. 0.1 M were prepared free of Cl_2, by oxidizing concentrated aqueous solutions of $NaClO_2$ (80% w/w, Aldrich) with $K_2S_2O_8$ (p.a. Merck) at 30°C. The gaseous OClO was carried away by an N_2 stream and collected in water at 0°C after being successively washed with aqueous solution of $NaClO_2$ and neat water. Stock solutions were kept frozen in brown bottles and were diluted under N_2 just before their use. Concentrations of OClO, from 1 to 20 mM were determined by absorption UV-Visible spectrophotometry at $\lambda = 359$ nm. The decadic absorption coefficient was determined by calibrating with aqueous solutions of OClO which were titrated by standard iodimetric methods [16, 17]: $\varepsilon_{359} = 1277\ \mathrm{M}^{-1}\mathrm{cm}^{-1}$.

2.2 OClO EPR Measurements

The cylindrical quartz cell containing OClO aqueous solution was placed in the optical transmission cavity TE_{103} of a Bruker ER 200 D X-band EPR spectrom-

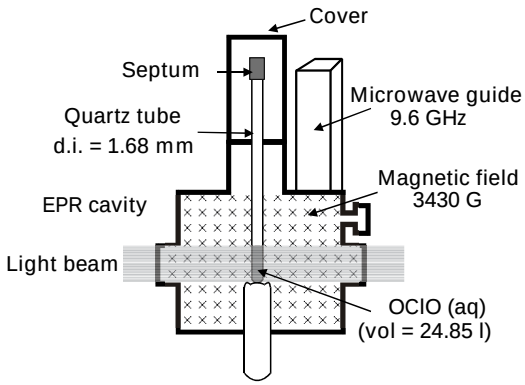

Fig. 1. Sample in a cylindrical cell irradiated in an EPR cavity.

eter. OClO is a stable radical, which gives specific EPR signal providing a continuous measurement of the progress of its photodecomposition (Fig. 1).

The EPR spectrum of OClO in aqueous solution at room temperature is partially resolved in a quartet as it is expected from the spin $S = 3/2$ of both isotopes ^{35}Cl and ^{37}Cl. However, when the EPR spectrum is recorded with a 16 G peak-to-peak modulation amplitude, sensitivity improves but resolution is lost and a singlet is obtained for the OClO spectrum in aqueous solution (Fig. 2). Larger modulation amplitudes induce strong distortion of the signal. During the photolysis, averaged sets of 10 spectra were scanned at regular time intervals with a constant gain until the signal vanished. The total acquisition time of each record

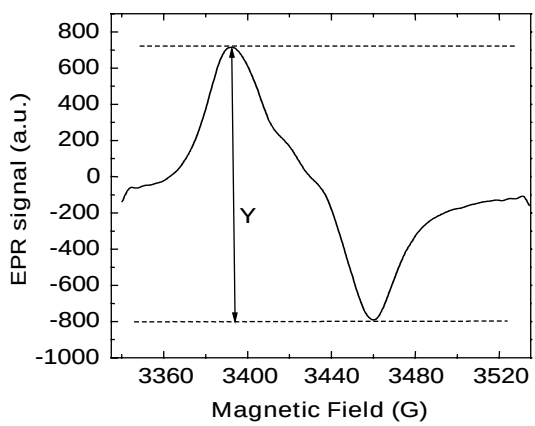

Fig. 2. First derivative X-band EPR spectrum of OClO in aqueous solution recorded with 16 G peak to peak field modulation. Microwave frequency, 9.56 GHz; microwave power, 18.0 mW; gain, $8 \cdot 10^4$; time constant, $2 \cdot 10^{-2}$ ms; scan time, 100 ms.

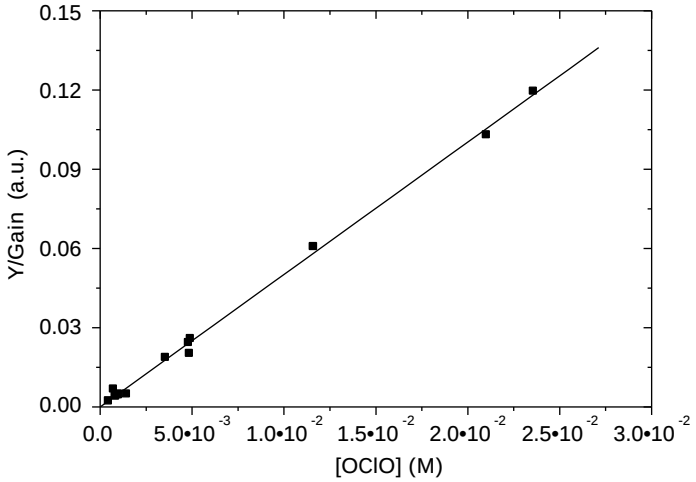

Fig. 3. Linearity of OClO EPR signal intensity with concentration. When dividing Y by the work gain g, the data fit to $Y/g = (5.016 \pm 0.061)$ [OClO], with correlation coefficient 0.9989 and standard deviation 0.00213.

was about 2 s, which is negligible in comparison with the total time of photolysis (~900 s).

Linearity of OClO EPR signal intensity Y_{OClO}, with OClO concentration was experimentally verified in the range of concentrations used in this work (Fig. 3). Interference from intermediate radicals such as ClO, Cl or ClO_3 was discarded because of their low concentrations in this system [18].

2.3 Irradiation Set Up and Actinometry

A Philips HPA 400 medium-pressure metal halide lamp with iron and cobalt additives was used as irradiation source. The lamp emits radiation mainly between 300 and 400 nm with an emission maximum at 366 nm. Monochromatic radiation of 366 ± 5 nm was isolated with a bandpass filter (Omega). The set was fixed to the EPR spectrometer in line with the optical transmission path of the cavity. A cylindrical photolysis cell made from quartz commercial tubing with internal (r) and external (R) radii of 0.8397 and 1.610 mm respectively, was used. The cell radii were carefully determined since they are considered when calculating the absorbent properties of the system.

A solution of potassium ferrioxalate ca. 0.15 M was employed as chemical actinometer. In order to make the analytical determination of the product possible, such a high concentration of the actinometer was used for two reasons: the small volume of irradiated solution (24.85 μl) and the recommended actinometer chemical conversion (less than 5%) [19]. We considered the amount of ferrous ions produced at 366 nm according to $\Phi = 1.20$ [20]. The concentration

of ferrous ion was spectrophotometrically determined by absorption at 510 nm of the 1-10-phenanthroline complex. Addition of 1 M NaF solution enabled us to avoid errors arising from slow colour development [21]. The decadic absorption coefficient of the Fe(II)-phenanthroline complex was obtained by calibrating at 510 nm: $\varepsilon_{510} = 11310\ M^{-1}cm^{-1}$.

On the basis of the low concentration of OClO solutions used in this work, their refractive indices at 366 nm were taken as that of neat water: $n_s = 1.34709$. The refractive indices at 366 nm of air and fused quartz, were calculated from the Cauchy equation [22]: $n_a = 1.00028$, $n_q = 1.47455$. The refractive index of potassium ferrioxalate 0.15 M solution was measured at 589 nm and corrected to 366 nm: $n_{act} = 1.354$. Absorbance measurements were carried out in 0.1 and 1 cm path length cells with a double-beam Shimadzu spectrophotometer.

2.4 Determination of Initial Rates of OClO Photodecomposition at 366 nm

The decay of the concentration of OClO in aqueous solution by irradiating with 366 nm light shows a complex kinetic as it can be observed in Fig. 4. Decay curves of the intensity of the OClO EPR signal Y_{OClO} vs. time t were obtained at different initial concentrations of OClO and fitted by polynomials of variable degrees, $Y(t) = a_0 + a_1t + a_2t^2 + ... + a_nt^n$. The initial record, which was obtained without irradiating, allowed for conversion of EPR signal units into concentration units. Considering the lineal relationship verified between signal intensity and OClO concentration: $Y_{OClO} = K[OClO]$, with K as the proportionality con-

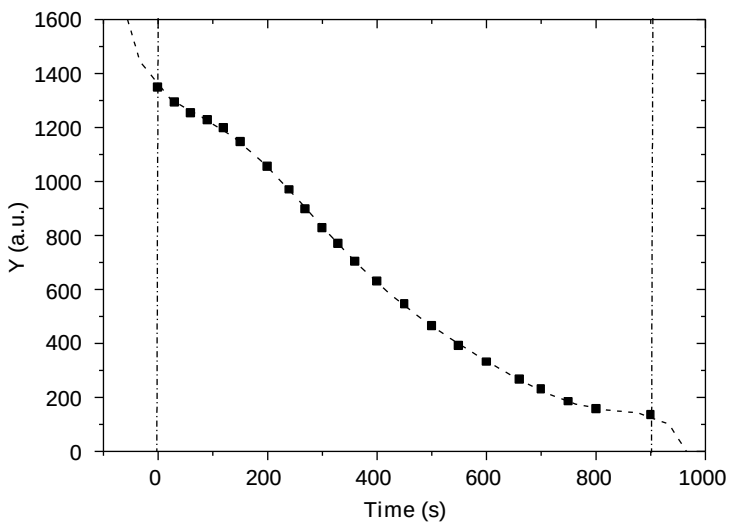

Fig. 4. Experimental data under N_2. OClO EPR signal Y_{OClO} vs. time irradiated at 366 nm; $[OClO]_0 = 6.6 \cdot 10^{-3}$ M. The decay curve was fitted with a seventh-order polynomial.

stant, the following equations arise for the initial rate of OClO photodecomposition:

$$\frac{\mathrm{d[OClO]}}{\mathrm{d}t} = \frac{1}{K}\frac{\mathrm{d}Y_{\mathrm{OClO}}}{\mathrm{d}t}, \qquad K = \frac{a_0}{[\mathrm{OClO}]_0}, \tag{4}$$

$$-v_0 = \left.\frac{\mathrm{d[OClO]}}{\mathrm{d}t}\right|_{t=0} = \frac{[\mathrm{OClO}]_0}{a_0}\left.\frac{\mathrm{d}Y_{\mathrm{OClO}}}{\mathrm{d}t}\right|_{t=0} = \frac{[\mathrm{OClO}]_0}{a_0}a_1 . \tag{5}$$

In all cases, the initial concentration $[\mathrm{OClO}]_0$ was determined spectrophotometrically at 359 nm, and the initial rate v_0 ($\mathrm{M \cdot s^{-1}}$) was calculated from a_0 and a_1 as shown in Eq. (5).

3 Theoretical Treatment for the Absorbed Photon Flow in a Cylindrical Cell

In order to determine quantum yields, absorbed photon flows have to be evaluated. The simplest way to measure the absorbed photon flow by chemical actinometry requires matching the absorbances of the reactant and the actinometer. In addition, even assuming constant intensity of the incident light, the respective refractive indices should be similar one to another in order to obtain identical fraction of reflected light. However, when matching absorbances, the chemical change in the actinometer may not be analytically measurable. In this case, a more suitable option is the employment of a concentrated solution of the actinometer. Thus, the incident photon flow P_0 must be related to the absorbed photon flow P_a and therefore, it is necessary to consider the optical properties of both the reactant and the actinometer solutions.

When the fraction of incident light that is transmitted and reflected at the different interfaces in a thick wall cylindrical cell is evaluated, the following assumptions should be introduced.

1. The tube is perfectly cylindrical. Surface irregularities and the small hemispherical base are neglected.

2. The incident beam is uniform and composed of parallel rays.

3. The light is monochromatic and “not polarized”. That means that it can be described as two beams of identical intensity, which are linearly polarized in orthogonal planes, arbitrarily chosen as the incidence and the perpendicular ones.

4. Air and quartz are assumed as transparent media.

5. The refractive index n must be replaced by the complex refractive index η, which depends on n, κ (Napierian molar absorption coefficient), C (concentration) and λ (wavelength): $\eta = n(1 + \mathrm{i}\kappa C\lambda/4\pi)$. Even though the solution absorbs light, reflection laws and Fresnel equations are valid because the imaginary component of the refractive index is negligible in comparison to the real component [23].

6. Absorption of light occurs only in the solution. The fraction of incident light that is absorbed can be derived from the Beer-Lambert law, since concentration can be considered uniform and constant under initial conditions.

Two classes of rays are considered in the following analysis. A zero-order ray EFG, is a ray that enters the solution arising from the lamp. Three first-order rays enter the solution originated by a first reflection at points F, G, E″. They are represented by FE′F′G′, GE″F″H″ and GH (Fig. 5). β and β' are the incidence angles of the generic ray EFG at points E and F. The ray defines the angles γ and γ' when entering the quartz and the solution respectively. Finally, when the ray leaves the solution, the angles are again β' and γ' at a point G in the interface solution-quartz. Assuming the constant incident photon flux I_0 (quanta $\cdot$ s^{-1}m^{-2}), the fraction of light that enters the solution is calculated by considering the Fresnel coefficients for light transmission at points E and F (T_E and T_F): $I_0 T_E T_F$. Notice that T_E and T_F depend on the incidence angles β and β' and on the refractive indexes of air n_a, quartz n_q, and solution (or actinometer) n_s (see appendix).

By applying the Lambert-Beer law to a zero-order ray EFG, the following equation arises:

$$I_a = I_0 T_E T_F [1 - \exp(-\kappa C L)] = I_0 f_0 . \tag{6}$$

Here L = FG, is the path length in the solution; and f_0 is defined as a zero-order absorption factor. L, T_E and T_F depend on z, with z being the variable incidence distance taken from the ray with normal incidence ($z = 0$). The maximum z corresponds to the ray that enters tangent to the interface quartz-solution, which has null path length in the solution. The path length in the solution $L(z)$ can be

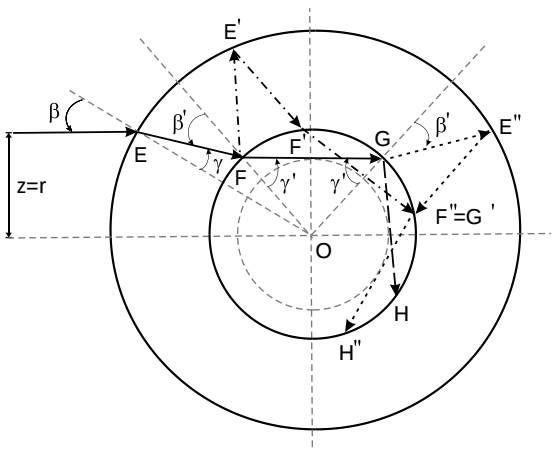

Fig. 5. Section of the cylindrical photolysis cell. A generic zero-order beam EFG, with $z = r$ is shown in full line; the three generic beams originated in a first reflection, FE′F′G′, GE″F″H″ and GH, are shown in dotted lines.

derived by trigonometric relation in an isosceles triangle OFG, when considering a generic zero-order ray EFG in Fig. 5.

$$L = 2r\cos\gamma' = 2r\sqrt{1-\sin^2\gamma'}\,, \tag{7}$$

$$\sin\beta = z/R\,. \tag{8}$$

By the Snell laws:

$$n_a \sin\beta = n_q \sin\gamma\,, \tag{9}$$

$$n_q \sin\beta' = n_s \sin\gamma'\,. \tag{10}$$

By using the sine rule in the triangle EFO [24, p. 51]:

$$\sin\beta'/\sin\gamma = R/r\,. \tag{11}$$

Replacing the equations above in Eq. (7), the path length is given by:

$$L = 2r\sqrt{1-(n_a/n_s)^2(z/r)^2}\,. \tag{12}$$

Since β, γ, β', and γ' are acute angles, their sinus vary between 0 and 1 and the following restrictions for z are obtained from Eqs. (8) to (11):

$$|z| \le R\,, \tag{13}$$

$$|z| \le (n_q/n_a)R\,, \tag{14}$$

$$|z| \le (n_q/n_a)r\,, \tag{15}$$

$$|z| \le (n_s/n_a)r\,. \tag{16}$$

The absorbed photon flow of a zero-order beam (without considering the reflections) P_a^0, is calculated by the definition in Eq. (6) and integration on z, as follows:

$$P_a^0 = \int_{-z_m}^{+z_m} I_a h\,dz = I_0 h \int_{-z_m}^{+z_m} f_0\,dz = I_0 h F_0\,, \tag{17}$$

with h being the height of the solution in the cell and F_0 the zero order absorption integral. The limits of integration $\pm z_m$, are given by the smallest z in Eq. (12). When $n_s < n_q$:

$$\pm z_m = \pm(n_s/n_a)r\,. \tag{18}$$

When reflections FE′F′G′, GE″F″H″ and GH are considered, one should notice that a zero-order ray and the first order rays arising from its reflections have the same path length. This property simplifies the problem notably, since the path lengths depend only on z as it may be seen in Eq. (12). The path lengths FG and GH are equal due to the equality between the angles FGO and HGO (γ') in the triangles OGH and OFG (reflection law). Similarly, equality of the path lengths for the remaining reflections may also be deduced:

$$\mathrm{FG} = \mathrm{GH} = \mathrm{F'G'} = \mathrm{F''H''} . \tag{19}$$

When considering reflections at the walls of the cell, the Fresnel coefficients R_E, R_F, T_E and T_F need to be evaluated. A first-order factor of absorption f_1 can be introduced as a correction factor because L is common to all the rays with the same z. Then, the total absorbed photon flux (see appendix), is given by:

$$I_a = I_0 f_0 \{1 + [(R_F + T_F^2 R_E)\exp(-\kappa CL) + R_E R_F]\} = I_0 f_0 (1 + f_1) . \tag{20}$$

Each one of the three first-order reflected rays considered in f_1 contributes differently to the absorbed photon flow, depending on the concentration of the solution. When assumption 3 is taken into account and the dependence of the Fresnel coefficients with light polarization is considered, the complete expression for the absorbed photon flow is given by:

$$P_a = I_0 h \frac{1}{2}\left\{\int_{-z_m}^{+z_m} f_{0\|}(1 + f_{1\|})\mathrm{d}z + \int_{-z_m}^{+z_m} f_{0\perp}(1 + f_{1\perp})\mathrm{d}z\right\}, \tag{21}$$

where $f_{\|}$ and $f_{\perp}$ denote the absorption factors for linearly polarized light in parallel and perpendicular directions to the incidence plane, respectively. The absorption integrals F_0 and F_1, may be obtained numerically by using computer programs to evaluate integrals by numerical calculation. Since the integrands are even functions of z, it follows that:

$$F_0 = \int_0^{+z_m} (f_{0\|} + f_{0\perp})\mathrm{d}z , \tag{22}$$

$$F_1 = \int_0^{+z_m} (f_{0\|} f_{1\|} + f_{0\perp} f_{1\perp})\mathrm{d}z . \tag{23}$$

The integrands of Eqs. (22) and (23), f_0 and $f_0(1 + f_1)$ are represented in Fig. 6 for [OClO] = 0.001 M, when the solution is irradiated at 366 nm ($\kappa_{366} = 2818$ $\mathrm{M^{-1}cm^{-1}}$). If reflections of superior orders are considered, the property of equal path lengths as exclusive function of z, continues being valid. We observed that the number of rays that should be considered in reflections of successive orders,

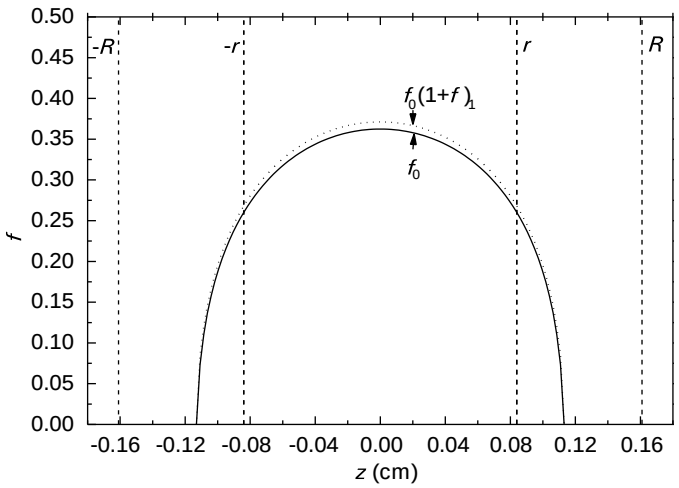

Fig. 6. f_0 and $f_0(1 + f_1)$ vs. z, calculated data for 366 nm, $[OClO]_0 = 10^{-3}$ M; $F_0 = 0.06632$ and $F_1 = 0.06825$.

is given by alternate terms in the Fibonacci sequence [24, p. 146]: 3, 8, 21, 55, etc. for first-, second-, third-, and fourth-order reflections. However, it can be concluded from previous results that corrections due to reflections of superior orders are unnecessary, at least in the exemplified system. Finally, one should observe that the cell of parallel plane faces becomes a particular case of the cylindrical tube irradiated perpendicularly to its axis when $z = 0$ in Fresnel equations.

4 Application to the Calculus of Quantum Yield of OClO Solutions

When considering Eq. (21) to evaluate the absorbed photon flow P_a, both the incident photon flux I_0 and the height of the solution in the cell h, are equal for OClO and actinometer solutions, and consequently the following relation is deduced:

$$I_0 h = \frac{P_{a\,act}}{(F_0 + F_1)_{act}} = \frac{P_{a\,OClO}}{(F_0 + F_1)_{OClO}} . \tag{24}$$

The absorbed photon flow $P_{a\,OClO}$ can be determined from Eq. (24) by measuring the absorbed photon flow for the ferrioxalate actinometer and calculating the integrals of zero- and first-order F_0 and F_1 for both solutions. The initial differential quantum yield for the 366 nm OClO photodecomposition in aqueous solution can be obtained from the slope of a plot of $-Vv_0$ (rate of conversion) vs. $P_{a\,OClO}$ according to the definition given in Eq. (3). Initial rates under dark con-

ditions must be considered in order to correct for thermal decomposition or evaporation of OClO in the tube.

5 Results and Discussion

According to Eq. (3), the plot in Fig. 7 gives the value for the initial differential quantum yield of OClO photodecomposition in aqueous solution $\Phi_{366} = 0.55 \pm 0.04$.

The quantum yield determined in this work considers the global process of photolysis, where the photofragments escaping from the solvent cage can participate in later chemical reactions. There are only few antecedents of determinations of global quantum yields of photolysis of OClO in aqueous solution. The values reported are larger than that obtained in this work at 366 nm. In 1932 Bowen and Cheung [25] obtained a 366.5 nm photolysis quantum yield value of 0.75 with $[OClO]_0 = 8.7 \cdot 10^{-3}$ M and $1.36 \cdot 10^{-2}$ M in aqueous solution. Years later, Buxton and Williams [26] reported 0.65 as the quantum yield of photolysis at 365 nm in pH 10 OClO solution. We obtained larger values for the initial differential quantum yield by increasing $[OClO]_0$ (Table 2). However, the results under these conditions were erratic probably due to the formation of bubbles from gaseous products, which affect the homogeneity of the system.

Quantum yields of OClO in carbon tetrachloride at 303, 365 and 436 nm have been determined in our laboratory by EPR spectrometry [27, 28]. However, the fraction of reflected light was not considered. In this case, the correction would be negligible since the refractive index of carbon tetrachloride is almost equal to the refractive index of quartz. We observed that the fraction of incident light

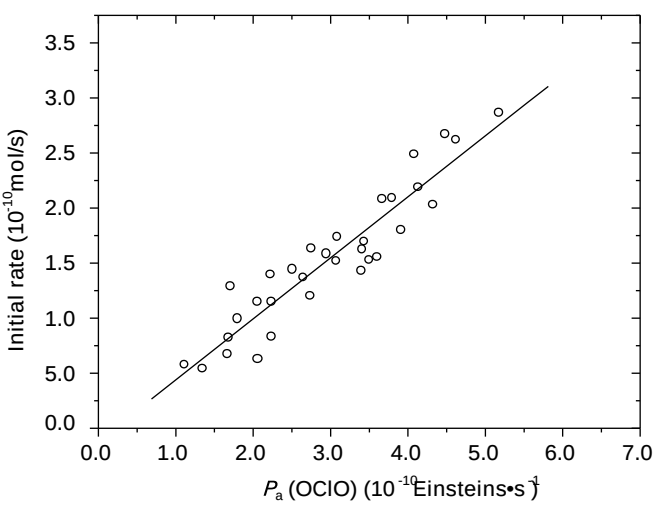

Fig. 7. Initial rates of conversion $(-Vv_0)$ of OClO 366 nm photodecomposition under N_2 vs. absorbed photon flow $P_{a\,OClO}$. The slope is the initial differential quantum yield.

Table 2. Initial differential quantum yield calculated from Eq. (22) for photolysis at 366 nm of concentrated solutions of OClO. $F_{OClO} = F_0 + F_1$; $F_{act} = 0.21283$; $V = 24.85$ μl.

[OClO] (M)	$P_a \cdot 10^{10}$ (Einsteins $\cdot$ s^{-1})	$-v_0 \cdot 10^6$ (M $\cdot$ s^{-1})	F_{OClO} (cm)	Φ (mol $\cdot$ Einsteins^{-1})
0.0132	4.073	8.66	0.2087	0.539
0.0166	4.433	10.71	0.2107	0.606
0.0223	3.430	15.25	0.2120	1.109
0.0236	4.298	16.15	0.2121	0.937
0.0249	5.280	26.33	0.2123	1.242

reflected at an interface increases with the difference between the refractive indices. In general, corrections due to the reflected light are more important in gaseous systems than in liquid ones. The refractive indices of gases and solids differ from each other more than the refractive indices of liquids and solids. As an example, we compared the fraction of reflected light of 0.001 M OClO aqueous solution and gaseous OClO in nitrogen (total pressure $=1$ atm) keeping constant the product κC. In the first case the difference $F_1 - F_0$ was 2.83% of F_1 while in gaseous solution, the same relation was 5.29%.

Attention should be paid to the spatial inhomogeneity effects in photochemical systems. These effects arise from high concentrations or high molar absorption coefficients of the light absorbing species which may originate inhomogeneous illumination across the sample. In our work, the measurements at initial conditions warrant homogeneous composition and physical properties of the system. However, effects of spatial inhomogeneous absorption of light may still take place. One should expect no effect from inhomogeneity of light absorption when the primary photoprocess only implies the formation of products which are transparent or inert towards reactant molecules [29]. For kinetically more complex photochemical reactions, the quantum yield Φ can vary with the reactant concentration, depending on the reaction mechanism. In this case the spatial distribution of the relevant species within the reactor should be taken into account.

Under the conditions of our measurements, the initial differential quantum yields for photodecomposition of aqueous solutions of OClO is constant within the considered concentration range, thus we found no evidence of such complexity or significant inhomogeneity effects beyond the experimental error (see Fig. 7).

Figure 8 shows the decay curves of OClO photolyzed in the EPR cells which are described in Table 1. Although the initial concentration of OClO is the same in the three experiments, different EPR signal profiles are obtained because the sample volume in the cavity is not the same in each case. Furthermore, the light path lengths are different in the three cells. In consequence, the photodecomposition rates are not directly comparable. However, it is possible to identify the interference of diffusion in the time evolution of the signal, masking the actual photolysis kinetics. Only in the case of the cylindrical cell the signal falls readily to zero as the photolysis proceeds. For the flat cells, the signals vanish much

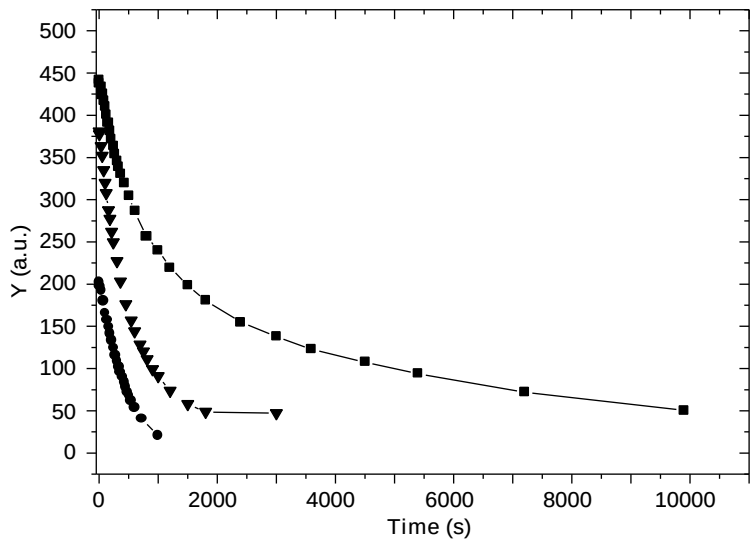

Fig. 8. Photodecomposition decay at 366 nm of OClO aqueous solution carried out under the same experimental conditions except for the photolysis cells. The different cells are described in Table 1. $[OClO]_0 = 3.35 \cdot 10^{-3}$ M. (●) cylindrical cell; (■) flat cell WG-813; (▼) flat cell WG-808.

more slowly in a way that may be explained only if considering diffusion processes and a large background signal. The contribution of OClO diffusion into the irradiated zone of the cavity from solution portions which are detected with less sensitivity [30, 31], seems to be particularly important in the case of the flat cell WG-813. On the contrary, the whole sample in the cylindrical cell is irradiated and it is reproducibly positioned in the middle of the cavity (Fig. 1).

6 Conclusions

The method developed in this work is applicable for quantitative photochemical studies on solutions of paramagnetic substances in cylindrical cells under the assumption of a lineal relationship between the EPR signal intensity and the concentration of the detected species.

In order to determine absorbed photon flows, the procedure does not require matching absorbances and refractive indexes of the reactant and actinometer. Moreover, any actinometer may be used even those showing physicochemical properties not comparable to the reactant. Solvents, solution volumes, cell diameters, or thickness of the cell walls may be varied from sample to actinometer providing total illumination and constant incident photon flux I_0.

The mathematical complexity in the evaluation of the absorbed photon flow is compensated with the advantages arising from the employment of a cylindrical quartz tube for aqueous solutions. Such a cell requires very small sample

volumes and the full sample in the cavity is irradiated. In fact, the thick walls in the tube avoid dark regions in the solution. For $n_s < n_q$ relation of refractive indices (this work), the external radius R must be larger than the internal radius r in n_s/n_a. On the other hand, when $n_s > n_q$, then $R > (n_q/n_a)r$.

Finally, the comparison of cylindrical and flat cell shows that the masking of the actual photochemical kinetics by diffusion processes is more likely avoided when using the former design.

Appendix. Fresnel Coefficients

The expressions for the Fresnel coefficients of transmission and reflection for non-perpendicular incidence differ according to the polarization of the light:

$$T_{E\perp} = \frac{4n_a n_q \cos\beta \cos\gamma}{(n_a \cos\beta + n_q \cos\gamma)^2}, \qquad T_{E\parallel} = \frac{4n_a n_q \cos\beta \cos\gamma}{(n_q \cos\beta + n_a \cos\gamma)^2}, \tag{A1}$$

$$T_{F\perp} = \frac{4n_q n_s \cos\beta' \cos\gamma'}{(n_q \cos\beta' + n_s \cos\gamma')^2}, \qquad T_{F\parallel} = \frac{4n_q n_s \cos\beta' \cos\gamma'}{(n_s \cos\beta' + n_q \cos\gamma')^2}, \tag{A2}$$

$$R_{E\perp} = \left(\frac{n_a \cos\beta - n_q \cos\gamma}{n_a \cos\beta + n_q \cos\gamma}\right)^2, \qquad R_{E\parallel} = \left(\frac{n_q \cos\beta - n_a \cos\gamma}{n_q \cos\beta + n_a \cos\gamma}\right)^2, \tag{A3}$$

$$R_{F\perp} = \left(\frac{n_q \cos\beta' - n_s \cos\gamma'}{n_q \cos\beta' + n_s \cos\gamma'}\right)^2, \qquad R_{F\parallel} = \left(\frac{n_s \cos\beta' - n_q \cos\gamma'}{n_s \cos\beta' + n_q \cos\gamma'}\right)^2. \tag{A4}$$

These equations are easily calculated as functions of z by considering Eqs. (8)–(11) in the main text:

$$\cos\beta = \sqrt{1 - \left(\frac{z}{R}\right)^2}, \qquad \cos\gamma = \sqrt{1 - \left(\frac{n_a}{n_q}\frac{z}{R}\right)^2}, \tag{A5}$$

$$\cos\beta' = \sqrt{1 - \left(\frac{n_a}{n_q}\frac{z}{r}\right)^2}, \qquad \cos\gamma' = \sqrt{1 - \left(\frac{n_a}{n_s}\frac{z}{r}\right)^2}. \tag{A6}$$

The coefficients from Fresnel equations at the points E, E′, and E″ on the external diameter are equal because the angles are symmetrically repeated when the ray leaves the solution. In the same way, the coefficients are equal at the points F, F′, F″, G, G′, H, H″ on the internal diameter.

The absorbed photon flux from each generic reflected ray is given by the following equations:

$$I_a(\mathrm{F'G'}) = I_0 T_E R_F R_{E'} T_{F'} j = I_0 f_0 R_E R_F \,, \tag{A7}$$

$$I_a(\mathrm{F''H''}) = I_0 T_E T_F \exp(-\kappa CL) T_G R_{E''} T_{F''} j = I_0 f_0 \exp(-\kappa CL) T_F^2 R_E \,, \tag{A8}$$

$$I_a(\mathrm{GH}) = I_0 T_E T_F \exp(-\kappa CL) R_G j = I_0 f_0 \exp(-\kappa CL) R_F \,. \tag{A9}$$

With $j = 1 - \exp(-\kappa CL)$, and f_0 the zero-order factor of absorption defined in Eq. (6). The total photon flux is the sum of Eqs. (A7) to (A9), and the total photon flow is:

$$P_a = I_0 h \int_{-z_m}^{+z_m} f_0[1 + R_E R_F + \exp(-\kappa CL) T_F^2 R_E + \exp(-\kappa CL) R_F] \mathrm{d}z \,. \tag{A10}$$

When light polarization is considered, the following equations are obtained by averaging the orthogonal components:

$$P_a = I_0 h \frac{1}{2} \left\{ 2 \int_0^{+z_m} f_{0\perp}[1 + R_{E\perp} R_{F\perp} + \exp(-\kappa CL) T_{F\perp}^2 R_{E\perp} + \exp(-\kappa CL) R_{F\perp}] \mathrm{d}z \right.$$

$$\left. + 2 \int_0^{+z_m} f_{0\|}[1 + R_{E\|} R_{F\|} + \exp(-\kappa CL) T_{F\|}^2 R_{E\|} + \exp(-\kappa CL) R_{F\|}] \mathrm{d}z \right\}, \tag{A11}$$

Replacing by f_1, the first-order factor of absorption defined in Eq. (20), we get:

$$P_a = I_0 h \left[\int_0^{+z_m} f_{0\perp}(1 + f_{1\perp}) \mathrm{d}z + \int_0^{+z_m} f_{0\|}(1 + f_{1\|}) \mathrm{d}z \right], \tag{A12}$$

After rearrangement, it finally results:

$$P_a = I_0 h \left[\int_0^{+z_m} (f_{0\perp} + f_{0\|}) \mathrm{d}z + \int_0^{+z_m} (f_{0\perp} f_{1\perp} + f_{0\|} f_{1\|}) \mathrm{d}z \right]. \tag{A13}$$

Acknowledgements

L. J. P. and M. S. C. thank Comisión de Investigaciones Científicas de la Provincia de Buenos Aires (CIC) and Consejo Nacional de Investigaciones Científicas y Técnicas (CONICET) respectively for supporting their work.

References

1. Jiany J.J.: Bruker Report **148**, 14–15 (2000)
2. Hunt R.E., Hill T.L.: J. Chem. Phys. **15**, 111–113 (1947)
3. Dignam M.J., Le Roy D.J.: J. Chem. Phys. **26**, 964–965 (1957)
4. Davies J.A., Manning P.P.: J. Am. Chem. Soc. **79**, 5148–5151 (1957)
5. Dunn R.C., Flanders B.N., Vaida V., Simon J.D.: Spectrochimia Acta **48A**, 1293–1301 (1992)
6. Zhang J., Aker P.: J. Phys. Chem. **98**, 765–767 (1994)
7. Bishenden E., Donaldson D.J.: J. Chem. Phys. **101**, 9565–9572 (1994)
8. Vaida V., Goudjil K., Simon J.D., Flanders B.N.: J. Mol. Liq. **61**, 133–152 (1994)
9. Vaida V., Simon J.D.: Science **268**, 1443–1448 (1995)
10. Roth M., Maul C., Gericke K.: J. Chem. Phys. **107**, 10582–10591 (1997)
11. Thøgersen J., Jepsen P.U., Thomsen C.L., Poulsen J.Aa., Byberg J.R., Keiding S.R.: J. Phys. Chem. A **101**, 3317–3323 (1997)
12. Hayes S.C., Philpott M.P., Mayer S.G., Reid P.J.: J. Phys. Chem. A **103**, 5534–5546 (1999)
13. Dunn R.C., Simon J.D.: J. Am. Chem. Soc. **114**, 4856–4860 (1992)
14. Thøgersen J., Thomsen C.L., Poulsen J.Aa., Keiding S.R.: J. Phys. Chem. A **102**, 4186–4191 (1998)
15. Mialocq J.C., Barat F., Gilles L., Hickel B., Lesigne B.: J. Phys. Chem. **77**, 742–749 (1973)
16. Nagai Y., Goodeve C.F.: Trans. Faraday Soc. **27**, 508–515 (1931)
17. Ingols R.S., Ridenour G.M.: J. AWWA **1948**, 1207–1227.
18. Adrian F.J., Bohandy J., Kim B.F.: J. Chem. Phys. **85**, 2692 (1986)
19. Kuhn H.J., Braslavsky S.E., Schmidt R., Pure Appl. Chem. **61**, 205 (1989)
20. Lee J., Seliger H.H.: J. Chem. Phys. **40**, 519–523 (1964)
21. Kirk A.D., Namasivayam C.: Anal. Chem. **55**, 2429–2431 (1983)
22. Lide D.R. (ed.): Handbook of Chemistry and Physics, 73rd edn., pp. 10–310. Boca Raton: CRC Press 1993.
23. Ditchburn R.W. (ed.): Light, 3rd edn. chapt. 15. London: Academic Press 1982.
24. Steiner E. (ed.): The Chemistry Maths Book. New York: Oxford University Press 1997.
25. Bowen E.J., Cheung W.M.: J. Chem. Soc. **1932**, 1200–1207.
26. Buxton G.V., Williams R.J.: Proc. Chem. Soc. **1962**, 141–142.
27. Churio M.S., Brusa M.A., Perissinotti L.J., Ghibaudi E., Coronel M., Colussi A.J.: Chem. Phys. Lett. **232**, 237–241 (1995)
28. Brusa M.A., Perissinotti L.J., Churio M.S., Colussi A.J.: J. Photochem. Photobiol. A **101**, 105–111 (1996)
29. Logan S.R.: J. Chem. Soc. Faraday Trans. **86**, 61–63 (1990)
30. Yordanov N.D.: Appl. Magn. Reson. **6**, 241–257 (1994)
31. Yordanov N.D., Ivanova M.: Appl. Magn. Reson. **6**, 347–357 (1994)

Authors' address: Luis J. Perissinotti, Department of Chemistry, University of Mar del Plata, Funes 3350, 7600 Mar del Plata, Argentina.